Quantifying Nitrogen-Vacancy Center Density in Diamond Using Magnetic Resonance

Morgan Hamilton

Center for Emergent Materials, Department of Physics, The Ohio State University, Columbus, OH

ABSTRACT

Biologists have recently began to consider the use of florescent nanodiamonds as candidates for conventional florescent biomarkers and in optical biolabeling. This is made possible by florescent defects in the crystal structure of the diamond, such as the nitrogen-vacancy (NV) center. The NV center is a color center, emitting bright red light upon excitation (with a green laser). In such applications as biolabeling, it is (useful/helpful/valuable) to be able to quantify the number of NV centers contained within a sample of nanodiamonds. Unfortunately, an accurate method of determining NV density in diamond is not yet available. We introduce a new potential method for quantifying NV density in a nanodiamond sample using magnetic resonance, in which the sample is placed inside a resonance cavity.

I. INTRODUCTION

I. Problems with Florescence-Related NV Density Measurements

Most diamond contains a certain natural concentration of NV centers. Previous work has taken advantage of spin-dependent luminescence to measure the density of NV centers in a nanodiamond sample. Unfortunately, it has been found that these optical measurements do not provide accurate results. One source of error involves the presentation of photoluminescence that is unrelated to diamond. For example, graphite shells and amorphous carbon may be present on the surface of the nanodiamonds, and each impurity may have its own fluorescence. In some cases, this surface fluorescence can be significantly greater than that of the color centers in the interior (1). Although precautions are taken in an attempt to process signals corresponding to the proper wavelength for NV emission, it is nearly impossible to filter out every signal arising from other defects and background noise.

II. Nitrogen Vacancy Centers

The nitrogen vacancy center is among the most common defects in diamond, consisting of a nitrogen substitution adjacent to a crystal lattice vacancy (1). Six electrons contribute to the electronic structure of the NV^- center: two from the nitrogen atom, one from each of the three carbon bonds surrounding the vacancy, and one which is captured from the lattice (1), resulting in the overall negative charge state. A visualization of the defect structure is shown in **Figure 1**.

The NV center is a spin triplet system ($S = 1$). In the absence of an external magnetic field, the $m_s = \pm 1$ spin-states are degenerate, with the $m_s = 0$ state naturally lower in energy. The energy difference between the $m_s = 0$ and $m_s = \pm 1$ states is called the zero-field splitting, given as $D = 2.87$ GHz (**Figure 2**). With application of an external magnetic field B_0, the degeneracy between the $m_s = \pm 1$ states is lifted, and the energies of the two spin-states split

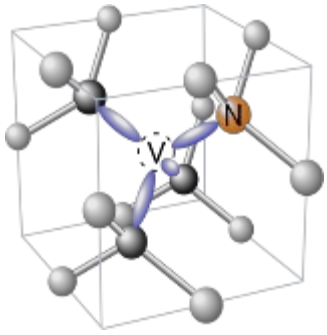

Figure 1

Nitrogen vacancy center in a crystal lattice. Ref. (7).

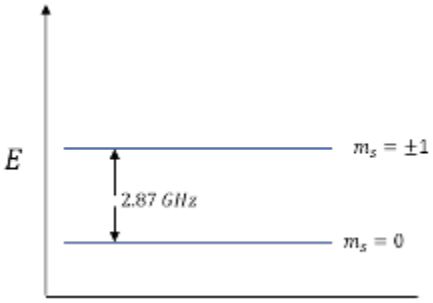

Figure 2

Zero-field splitting of spin states in NV⁻ at 2.87GHz.

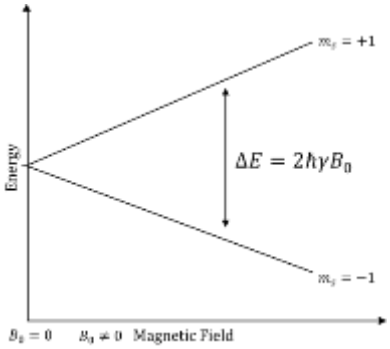

Figure 3

Zeeman splitting of NV⁻ $m_s = \pm 1$ spin states due to application of external magnetic field.

relative to 2.87GHz, with the $m_s = +1$ state being higher in energy than the $m_s = -1$ state. The states are then separated in energy by $\Delta E = 2\hbar\gamma B_0$ (**Figure 3)**, where γ is the electron gyromagnetic ratio.

The NV center is a color center, exhibiting photoluminescence which can be identified optically by its emission and absorption spectra (1). This defect is unique among other color centers in it that it is magnetic, and furthermore that the florescence is coupled to the spin state (1). This allows for modulation of the luminescence intensity by magnetic fields, a property which can be exploited to monitor external magnetic and electric fields with great sensitivity and nanoscale resolution (1). This property of NV centers is of particular interest, as it lends itself to several exciting applications in physics and biology.

Alternatively to utilizing spin-fluorescence coupling to determine NV center density, one can perform magnetic resonance measurements on nanodiamond samples by coupling NV spins to microwaves inside a resonance cavity. The most basic experiment involves the use of a cavity with a strong resonance frequency equal to the zero-field splitting of the NV center. Microwaves are directed into the cavity at a steady frequency matching the zero-field splitting, and a magnet is used to sweep an external magnetic field over the resonance. Microwave absorption by the sample occurs when the applied microwave frequency matches the frequency of spin transitions, which are tuned into resonance using an applied magnetic field, B_0. The resulting EPR spectrum shows peaks with amplitudes corresponding to the microwave absorption intensity, and the integrated intensity is proportional to the concentration of NV centers in the sample.

II. Microwave Cavities

In its simplest form, a microwave cavity is a metal box with rectangular or cylindrical shape that confines electromagnetic radiation and uses resonance to amplify weak signals emitted from the sample placed inside. A microwave field is supplied to the cavity, and a frequency sweep is performed over the resonance. When this frequency matches a resonance frequency for the

cavity, standing waves are formed as a consequence. This implies that the electric and magnetic microwave (H_1) fields are entirely out of phase when the resonance condition is met, i.e. the antinode of one field corresponds to the node of the other. This is an important aspect of the resonance cavity; in a magnetic resonance experiment, optimal sample placement occurs within a magnetic field maximum, or equivalently, at an electric field minimum. It is possible to determine the approximate locations of these H_1 maxima by examining the cavity modes. This aspect will be discussed in more depth in §1.3 and §4.4.

The design of a resonance cavity is driven by the desire to create a mechanism which will amplify weak signals coming from a sample which are already emitted under resonance. There are several ways to characterize how effective a resonance cavity is in doing this. The quality factor (Q-factor) of a cavity is a measure of how efficiently the cavity stores microwave energy. A lower Q-factor implies that greater amounts of energy are being lost, and vice versa.

There are many ways that energy may be lost in a cavity. Commonly, energy is lost to the side walls of a cavity due to induced electrical currents in the metal which in turn generate heat (2). This energy loss can be minimized by using a highly conducting material for the cavity walls, such as copper, but some loss is inevitable as there are no truly perfect conductors. Another frequent way that energy is dissipated involves the coupling between the cavity and wave-carrier, where the two components may be over- or under-coupled. This will be discussed in more detail later in this section.

Assuming no energy is lost to additional external factors, the Q-factor depends on the cavity material, dimensions, and the particular mode which is being exited in the cavity at a given frequency. The theoretical Q-factor for a cavity of length *d*, height *a*, and width *b* with a corresponding mode of indices *l*, *m*, *n* is then given by the equation

$$Q = \frac{a\ b\ d\ k_r^3\ k_{xy}^2\ Z_0}{4R_s\left(a\ b\ k_{xy}^2\ k_z^2 + b\ d\left(k_{xy}^2 + k_y^2\ k_z^2\right)\left\{\begin{matrix}1/2 & l=0\\ 1 & \text{else}\end{matrix}\right) + a\ d\left(k_{xy}^4 + k_x^2\ k_z^2\right)\left\{\begin{matrix}1/2 & m=0\\ 1 & \text{else}\end{matrix}\right)\right)}, \quad (1.2.1)$$

where k_r is the wavenumber

$$\sqrt{k_x^2 + k_y^2 + k_z^2}\ , \quad (1.2.2)$$

and k_x, k_y, k_z are components of the wavevector k, given by

$$\left.\begin{matrix}\text{(i)}\quad k_x = m/a\\ \text{(ii)}\quad k_y = n/b\\ \text{(iii)}\quad k_z = l/d\end{matrix}\right\} \quad (1.2.3)$$

with $k_{xy} = \sqrt{k_x^2 + k_y^2}$.

The vacuum impedance, Z_0, is defined as the ratio $Z_0 = \frac{|\boldsymbol{E}|}{|\boldsymbol{H}|}$ and relates the magnitudes of the electric and magnetic fields of an electromagnetic wave propagating through a vacuum. It is a physical constant, approximately equal to $120\pi\ \Omega$.

To measure the Q-factor for a cavity at a particular frequency, a more useful definition is given by

$$Q = \frac{\nu_{res}}{\Delta\upsilon}, \tag{1.2.4}$$

where υ_{res} is the resonance frequency and $\Delta\nu$ is the full width at half maximum (FWHM) for that frequency (**Figure 4**) (2).

Figure 4

Reflected microwave power from a resonance cavity, showing the resonance frequency υ_{res} and FWHM, $\Delta\upsilon$. Ref. 2.

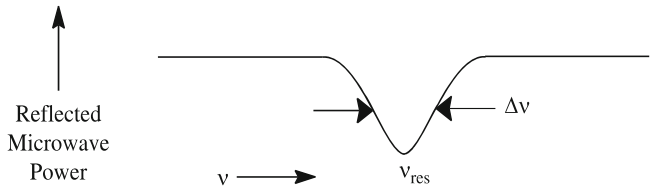

Another important aspect in the cavity design is the filling factor. The filling factor of a cavity, in essence, describes to what degree the sample fills the cavity. In an EPR measurement, it is the external magnetic field B_0 which drives absorption, ultimately creating the signal. More precisely, the filling factor indicates the degree to which the sample fills the region of the cavity in which B_0 is strong (3). If the applied magnetic field were uniform throughout the cavity, the filling factor would simply be the ratio of the sample volume to the resonator volume (3), but as this is not the case, the filling factor is rather given by

$$\eta = \frac{\int_{sample} B_0^2 dV}{\int_{cavity} B_0^2 dV}. \tag{1.2.5}$$

Therefore, it is favorable that the sample be commensurate in size with regions of strong magnetic field within the cavity.

An additional factor of importance is in the coupling between the cavity and the mechanism used to transfer microwaves into the cavity. This depends on the particular mechanism. A waveguide is a typical method of coupling microwaves into a resonance cavity, involving a hollow, conductive, metal tube which carries microwaves from the source to the resonator. Another option is a coaxial cable, which requires the use of an antenna to couple between the cable and cavity. Coupling between a microwave cavity and coaxial cable will be explored in more depth in §5.2. For either method, the degree of coupling depends largely on sufficient impedance matching between the cavity and wave-carrier. The coupling coefficient is defined as

$$\beta = \frac{R_0 n^2}{r}, \tag{1.2.6}$$

where R_0 is the impedance of the microwave source, n is the turns ratio for the transformer, and r is the impedance of the cavity (8). For a cavity which is critically coupled, or "matched," $\beta = 0$. In this case, there is maximum power transfer from the microwave source to the cavity, and no waves are reflected from the cavity (8). This results is maximum EPR sensitivity. For $\beta < 1$, the cavity is said to be undercoupled, resulting in reflection of microwaves from the cavity and a higher Q-factor than a matched cavity. The last case is for $\beta > 1$, in which the cavity is overcoupled. This also results in the reflection of microwaves from the cavity, but with a lower Q-factor than for a matched cavity (8).

III. Transverse Electric Modes (5)

This section outlines the derivation leading to the solutions for transverse electric modes propagating in a rectangular cavity.

For monochromatic waves propagating in the cavity, **E** and **B** have the generic form

$$\begin{aligned} &\text{(i)} \quad \boldsymbol{E}(x,y,z,t) = \boldsymbol{E}_0(x,y,z)e^{-i\omega t} \\ &\text{(ii)} \quad \boldsymbol{B}(x,y,z,t) = \boldsymbol{B}_0(x,y,z)e^{-i\omega t} \end{aligned} \tag{1.3.1}$$

Assuming that the cavity is a perfect conductor, it must be that $\boldsymbol{E} = \mathbf{0}$ and $\boldsymbol{B} = \mathbf{0}$ inside the material itself. Therefore, the above equations are constrained by the boundary conditions

$$\left.\begin{aligned} &\text{(i)} \quad \boldsymbol{E}^{\parallel} = \mathbf{0} \\ &\text{(ii)} \quad B^{\perp} = 0 \end{aligned}\right\} \tag{1.3.2}$$

at all surfaces. The electric and magnetic fields must satisfy Maxwell's equations within the cavity:

$$\left.\begin{aligned} &\text{(i)} \ \nabla \cdot \boldsymbol{E} = 0 \quad \text{(iii)} \ \nabla \times \boldsymbol{E} = -\frac{\partial B}{\partial t} \\ &\text{(ii)} \ \nabla \cdot \boldsymbol{B} = 0 \quad \text{(iv)} \ \nabla \times \boldsymbol{B} = \frac{1}{c^2}\frac{\partial E}{\partial t} \end{aligned}\right\} \tag{1.3.3}$$

The problem is then to find functions $\boldsymbol{E}_0$ and $\boldsymbol{B}_0$ such that the fields (3.1) satisfy the differential equations (3.3), constrained by the boundary conditions (3.2).

As confined waves are generally not transverse, one must include longitudinal components (E_z and B_z) in order to satisfy the boundary conditions:

$$\left.\begin{aligned} \boldsymbol{E}_0 &= E_x\hat{x} + E_y\hat{y} + E_z\hat{z} \\ \boldsymbol{B}_0 &= B_x\hat{x} + B_y\hat{y} + B_z\hat{z} \end{aligned}\right\} \tag{1.3.4}$$

where each of the components is a function of *y* and *z*. Putting (3.4) into Maxwell's equations (iii) and (iv), we obtain:

$$\left.\begin{array}{ll} \text{(i)} & \dfrac{\partial E_y}{\partial x}-\dfrac{\partial E_x}{\partial y}=i\omega B_z \\ \text{(ii)} & \dfrac{\partial E_z}{\partial y}-i\kappa E_y=i\omega B_x \\ \text{(iii)} & i\kappa E_x-\dfrac{\partial E_z}{\partial x}=i\omega B_y \end{array}\right\} \quad \left.\begin{array}{ll} \text{(iv)} & \dfrac{\partial B_y}{\partial x}-\dfrac{\partial B_x}{\partial y}=-\dfrac{i\omega}{c^2}E_z \\ \text{(v)} & \dfrac{\partial B_z}{\partial y}-i\kappa B_y=-\dfrac{i\omega}{c^2}E_x \\ \text{(vi)} & i\kappa B_x-\dfrac{\partial B_z}{\partial x}=-\dfrac{i\omega}{c^2}E_y \end{array}\right\} \tag{1.3.5}$$

Equations (ii), (iii), (v), and (vi) can be solved for E_x, E_y, B_x, and B_y:

$$\left.\begin{array}{ll} \text{(i)} & E_x=\dfrac{i}{(\omega/c)^2-\kappa^2}\left(\kappa\dfrac{\partial E_z}{\partial x}+\omega\dfrac{\partial B_z}{\partial y}\right) \\ \text{(ii)} & E_y=\dfrac{i}{(\omega/c)^2-\kappa^2}\left(\kappa\dfrac{\partial E_z}{\partial y}-\omega\dfrac{\partial B_z}{\partial x}\right) \\ \text{(iii)} & B_x=\dfrac{i}{(\omega/c)^2-\kappa^2}\left(\kappa\dfrac{\partial B_z}{\partial x}-\dfrac{\omega}{c^2}\dfrac{\partial E_z}{\partial y}\right) \\ \text{(iv)} & B_y=\dfrac{i}{(\omega/c)^2-\kappa^2}\left(\kappa\dfrac{\partial B_z}{\partial y}+\dfrac{\omega}{c^2}\dfrac{\partial E_z}{\partial x}\right) \end{array}\right\} \tag{1.3.6}$$

Then it is adequate to determine the longitudinal components E_x and B_x. When these are known, we can easily find all other components using (3.6). Inserting (3.6) into the remaining Maxwell equations gives uncoupled equations for E_z and B_z:

$$\left.\begin{array}{ll} \text{(i)} & \left[\dfrac{\partial^2}{\partial x^2}+\dfrac{\partial^2}{\partial y^2}+(\omega/c)^2-\kappa^2\right]E_z=0 \\ \text{(ii)} & \left[\dfrac{\partial^2}{\partial x^2}+\dfrac{\partial^2}{\partial y^2}+(\omega/c)^2-\kappa^2\right]B_z=0 \end{array}\right\} \tag{1.3.7}$$

If $E_x=0$ we call these transverse electric (TE) waves, and if $B_x=0$ we call them transverse magnetic (TM) waves. If both $E_x=0$ and $B_x=0$, we call them transverse electromagnetic (TEM) waves.

For a cavity of rectangular shape (**Figure 5**) with height *a*, width *b*, and length *d* where we are interested in the propagation of TE waves, we must solve Eq. 3.7ii, subject to the boundary condition 3.2ii. This can be accomplished using separation of variables. Let

$$B_z(x,y,z)=X(x)Y(y)Z(x), \tag{1.3.8}$$

such that

$$YZ\frac{d^2X}{dx^2} + ZX\frac{d^2Y}{dy^2} + XY\frac{d^2Z}{dZ^2} + [(\omega/c)^2 - k^2]XYZ = 0 \tag{1.3.9}$$

Divide by XYZ, and take notice that the x-, y-, and z-dependent terms must be constants:

$$\left.\begin{array}{ll} \text{(i)} & \frac{1}{X}\frac{d^2X}{dx^2} = -k_x^2 \\ \text{(ii)} & \frac{1}{Y}\frac{d^2Y}{dy^2} = -k_y^2 \\ \text{(iii)} & \frac{1}{Z}\frac{d^2Z}{dz^2} = -k_z^2 \end{array}\right\} \tag{1.3.10}$$

with

$$-k_x^2 - k_y^2 - k_z^2 + (\omega/c)^2 - k^2 = 0. \tag{1.3.11}$$

The general solution to Eq. 3.10i is given by

$$X(x) = A\ sin(k_x x) + B\ cos(k_x x). \tag{1.3.12}$$

However, the boundary conditions require that B_x—and hence also (Eq. 3.6iii) dX/dx –goes to zero at $x = 0$ and $x = a$. Then it must be the case that $A = 0$ and

$$k_x = m\pi/a, \qquad (m = 0, 1, 2 \ldots). \tag{1.3.13}$$

Similarly for Y and Z,

$$k_y = n\pi/b, \qquad (n = 0, 1, 2 \ldots), \tag{3.14}$$

$$k_z = l\pi/d, \qquad (l = 0, 1, 2 \ldots). \tag{3.15}$$

Thus, we conclude that

$$B_z = B_0 \cos(l\pi z/d)\cos(m\pi x/a)\cos(n\pi y/b). \tag{3.16}$$

For electromagnetic waves confined to the interior of a cavity of length *d*, width *b*, and height *a* (**Figure 5**), solutions to the above equation are called TE_{lmn} modes, where the indices *l* ,*m*, *n* are integers indicating the quantization of the electric field in the corresponding dimension. The first index is conventionally associated with the larger dimension, so we assume that $d \geq a \geq b$. For a transverse electric (TE_{lmn}) mode, the cutoff frequency is

$$\omega_{lmn} = c\pi\sqrt{(l/d)^2 + (m/b)^2 + (n/b)^2}\,.$$

This is the lowest frequency at which the mode will propagate. The TE modes which propagate in a cavity therefore depend upon the applied microwave frequency and the cavity dimensions. **Figure 6** shows a visualization of a TE_{101} mode as an electric field density plot.

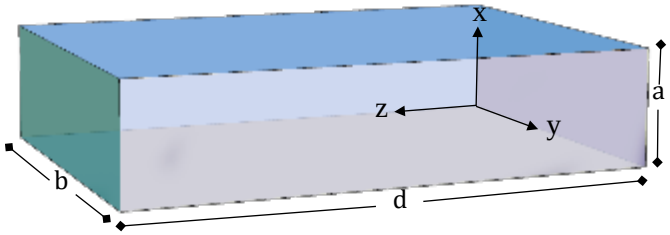

Figure 5

Microwave cavity concept with length d, width b, and height a.

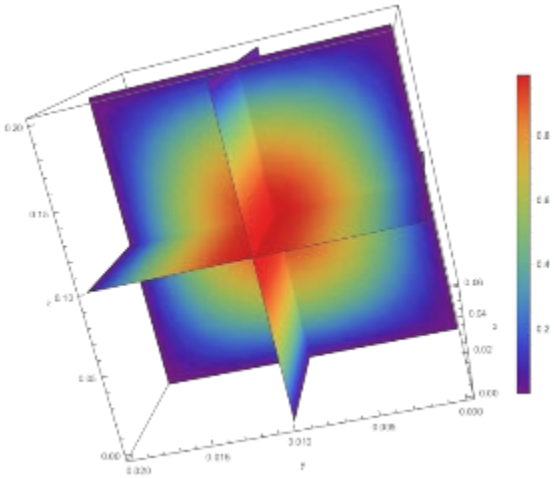

Figure 6

Visualization of TE_{101} mode in a rectangular cavity showing density plot of microwave electric field

IV. MATERIALS AND METHODS

I. Designing a Microwave Cavity: Powder Patterns

In order to perform resonance measurements on a nanodiamond sample, it was first necessary to design and machine a new microwave cavity. A variety of commercial cavities are available, but they are typically tuned to frequencies upwards of 9.0 GHz. While the resonance condition can still be met at this frequency, a problem arises in the quality of the EPR signals. A nanodiamond sample may contain a number of NV centers, for which there are four possible orientations that may be adopted by each defect for $m_s = \pm 1$. For a single nanodiamond, this results in clear EPR signals with eight distinct peaks (**Figure 7**). In this case, the eigenstates of the Hamiltonian are the eigenbasis and are hence diagonal, resulting in the linear dispersions seen in **Figure 3** for $m_s = \pm 1$. The basic Hamiltonian is given as

$$H = DS_z^2 + \gamma \boldsymbol{B}_0 \cdot \boldsymbol{S}, \tag{5.1.1}$$

where $\boldsymbol{B}_0$ is the applied magnetic field, $\boldsymbol{S}$ is the spin-1 operator, and D is the zero-field splitting. Diagonalization of the Hamiltonian yields the eigenstates, which are sensitive to the direction of the applied magnetic field and thus depend upon the angle φ between B_0 and the NV axis (6). In many-NV samples, the result of many possible orientations is the manifestation of so-called powder patterns. In this case, the eigenstates are no longer the eigenbasis and are not diagonal, and thus produce curved dispersions, as shown in **Figure 8**.

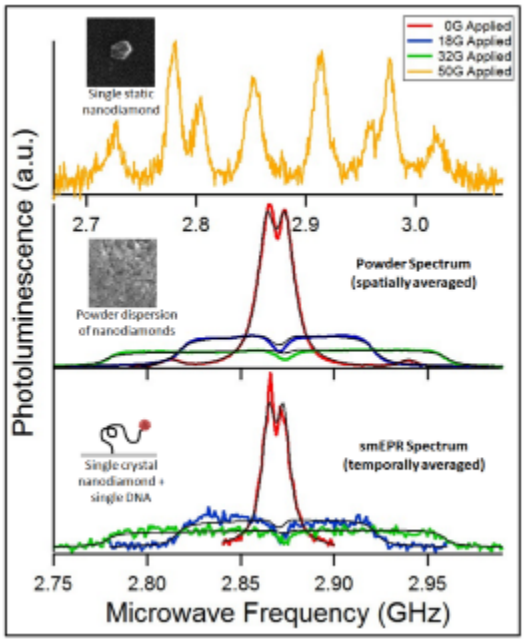

Figure 7

Result of powder dispersions in EPR spectrum with varying applied magnetic field intensities (b). Ref (6).

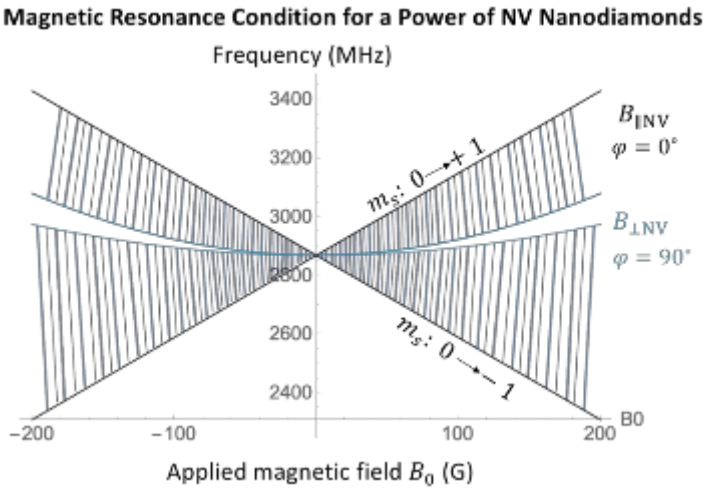

Figure 8

Splitting of $m_s = \pm 1$ spin state energies following application of magnetic field sweep, including powder patterns (blue) resulting from many NV orientations ($0° < \varphi < 90°$) in the sample.

II. Designing a Microwave Cavity: Physical Considerations

Three factors primarily drove the design of the microwave cavity: frequency, modes, and physical constraints. As discussed in §1.2, the formation of standing waves in the cavity is a consequence of resonance, and optimal sample placement for magnetic resonance measurements occurs within a magnetic field maximum and electric field minimum. It is convenient for this magnetic field antinode to occur at the center of the cavity for ease of sample placement and optimization of the filling factor. It is then desirable to excite a mode which provides a magnetic field maximum at the cavity center, and which propagates at a frequency very near the zero-field splitting of the NV center ($D = 2.87$ GHz).

Additional considerations in the cavity dimension lie in physical constraints from the electromagnet. As the magnetic field sweep is provided by an external magnet, it is required that the cavity fit within the bounds of that magnet. The physical constraints from this magnet (**Figure 9**) determine that it is necessary to have the height, $a < 6$ cm and the width, $b < 2$ cm, with no constraints on the cavity length. The mode which best fits these requirements is TE_{210} (**Figure 10**), for which the electric field is quantized twice along the length of the cavity, once along the height of the cavity, and is constant in the cavity width. The double quantization of the electric field along the cavity length implies an electric field node exactly at the center of the cavity. Because the electric field is constant in the y-dimension—along the cavity width— the mode frequency is independent of this dimension. Therefore, the width can be made as small as necessary. Conversely, because the cavity length is not restricted by the magnet, this dimension can be as large as necessary. Because there are no constraints on the cavity length, values were chosen for the cavity width, and using the desired frequency and

mode, the appropriate cavity length could be determined. For a rectangular cavity of length d, height a, and width b, with mode TE_{210}, the (linear) frequency is given by

$$f = \frac{c}{2}\sqrt{(l/d)^2 + (m/b)^2 + (n/b)^2} \tag{4.1}$$

This equation can be rearranged to describe the cavity height as a function of the length, as $n = 0$ for TE_{102}.

$$a(d) = \left[\left(\frac{2f}{c}\right)^2 - \left(\frac{2}{d}\right)^2\right]^{-\frac{1}{2}}$$

Plotting this function (**Figure 11**), reasonable dimensions can be chosen for the cavity height a and length d. For cavity dimensions $d = 21.2$ cm, $b = 2.0$ cm, $a = 6.0$ cm, the frequency of the TE_{210} mode is 2.87 GHz.

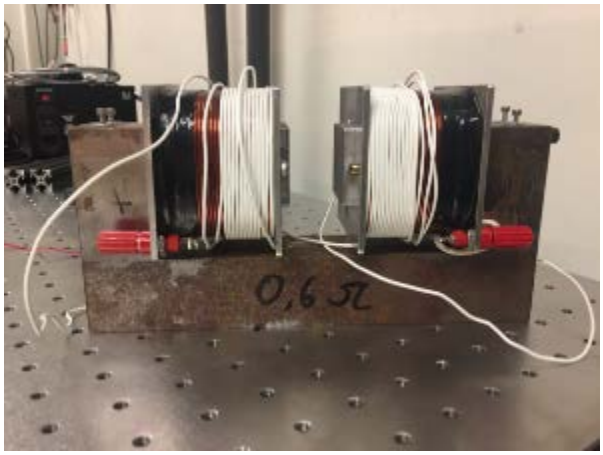

Figure 9

Electromagnet which will hold the microwave cavity and provide a magnetic field sweep. The white wire makes up the magnet modulation coils.

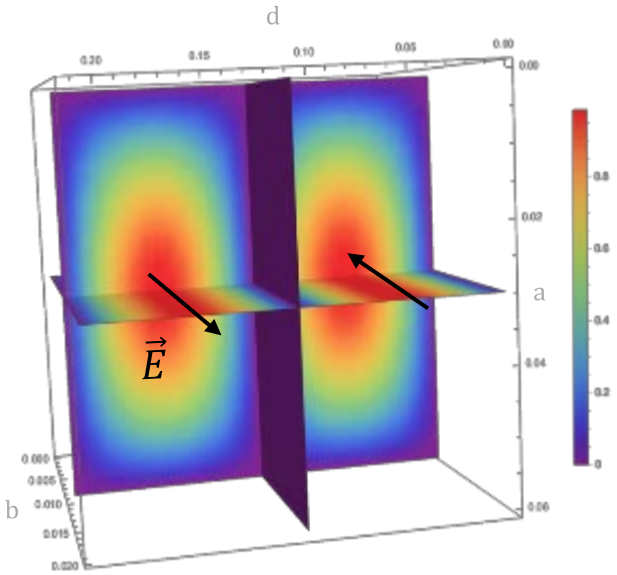

Figure 10

Visualization of TE_{210} mode showing density plot of the electric field. The changing direction of the E-field is shown by two example vectors (black), a consequence of standing wave formation via resonance.

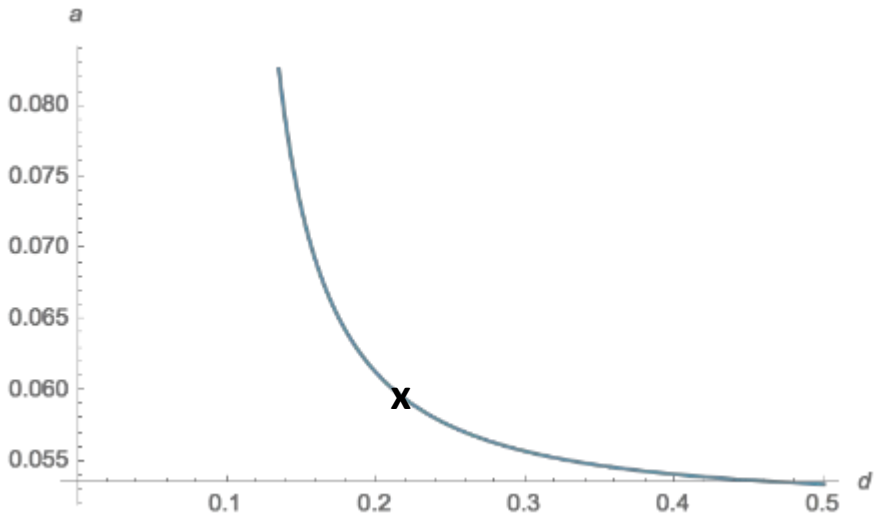

Figure 11

Height of resonance cavity as a function of the cavity length (m), following the relationship $a(d) = \left[\left(\frac{2f}{c}\right)^2 - \left(\frac{2}{d}\right)^2\right]^{-\frac{1}{2}}$. The "x" indicates the chosen solution for the cavity length and height.

III. Model Cavity

A model cavity (**Figure 12**) was used preliminarily in an attempt to investigate cavity modes and coupling with a coaxial cable before deciding on a final design for the microwave cavity. This model cavity was a rectangular, metal box constructed from an unknown, magnetic material. The dimensions consisted of length $d = 19.8$ cm, height $a = 5.5$ cm, and width $b = 11$ cm, making the model cavity similar to the proposed cavity design in the length and height dimensions. The box was fitted with an SMA connector, to which a copper wire was soldered for use as an antenna (**Figure 14**). The purpose of the antenna is to couple the cavity with the coaxial cable transmitting the microwaves. It was decided that the antenna should be loop-shaped over a vertical or stud antenna, as magnetic coupling was desired; a stud antenna drives the electric field rather the magnetic field. This is not the case for the loop shape, and it is a simple task to determine how it should be oriented within the cavity to couple with the desired mode, knowing that the magnetic field produced by the current flowing through the wire should be as in Figure X. To couple to the TE_{210} mode, the loop should be oriented in the XZ-plane.

The model cavity was connected to a VNA network analyzer, and a frequency sweep (0-27GHz) was performed. A sample peak from the resulting frequency spectrum is shown in **Figure 13**. This peak represents a weak resonance frequency at 2.055GHz. In order to quickly assess the resonance frequencies which appeared in the spectrum, a Java program was developed which calculates all possible TE modes for a given frequency and dimensions. The program also returns the cutoff frequency and theoretical Q-factor for each mode. **Figure 15** shows a sample of the program interface.

Figure 12

A view of the model cavity showing coordinate system and connection to a coaxial cable as the microwave transmission line.

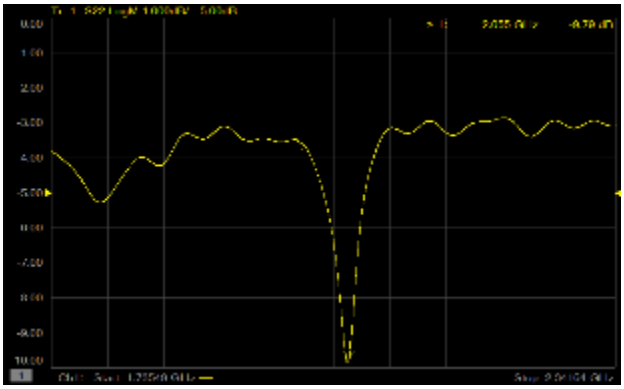

Figure 13

(Section) of frequency spectrum produced by VNA. A weak resonance at 2.055 GHz is shown.

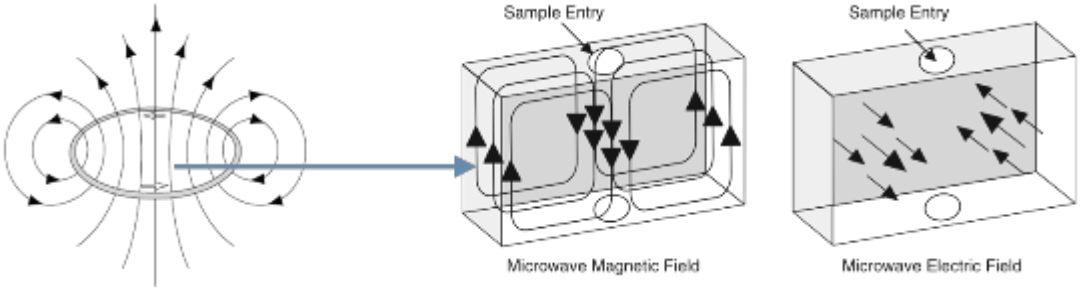

Figure 14

H_1 field generated by loop current couples with MW magnetic fields inside the cavity.

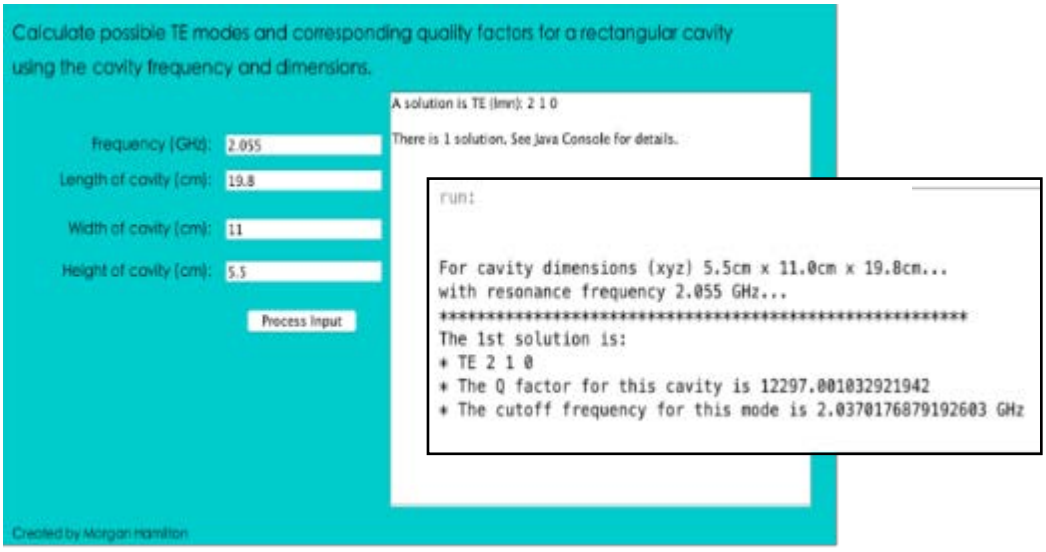

Figure 15

Program interface for Java mode calculator.

IV. Probing and Visualizing Transverse Electric Modes

To investigate the orientation of the electric and magnetic fields involved in a cavity mode, a simple probing method described by Richard Feynman in The Feynman Lectures (Vol. II, Ch. 23) was utilized. A small wire is inserted into the cavity through a hole along one of the cavity faces. If the alignment of the wire is parallel to the electric field, a current is induced in the wire, causing the resonance to disappear from view in the VNA spectrum. The reason for suppression of the resonance can be easily understood by examining Equation 1.2.4 for the Q-factor:

$$Q = \frac{\nu_{res}}{\Delta\upsilon}$$

As the resonance disappears, it is so that the Q-factor for the resonance rapidly decreases. As a current is induced in the wire, energy is sapped from the cavity and therefore the efficiency of microwave storage is decreased. For a constant resonance frequency ν_{res} and a decreasing Q, it must be that $\Delta\upsilon$ is increasing proportionally. This is the FWHM of the resonance, and so the effect is that of stretching the resonance peak horizontally until it can no longer be distinguished from the background. This probing method allows one a simple way to confirm the modes predicted by the Java program in §4.3.

It is convenient to be able to visualize the cavity modes, for both probing and to aid in the determination of optimal sample placement. For this purpose, a Mathematica program was created which allows the user to visualize any valid[1] TE mode for given cavity dimensions. The program returns the cutoff frequency for the mode as well as 3-dimensional density plots of the electric and magnetic fields involved in the mode. **Figure 16** shows a sample of the program interface.

Several holes were placed along the lid of the model cavity to investigate the modes using this probing method. At 2.055 GHz, the expected mode for the cavity dimensions is again, TE_{210} (**Figure 17**). For this cavity, the length is greater than the width, and both are greater than the height. Therefore, the first index corresponds to the cavity length, the second index corresponds to the cavity width, and the third index corresponds to the cavity height. The mode indices then indicate that the electric field is quantized twice along the cavity length, once along the cavity width, and not at all along the cavity height. This suggests that the electric field is constant along the cavity height. Therefore, it is expected that inserting a wire vertically through a hole in the top of the cavity should significantly disturb the resonance where there is an electric field antinode. This effect is shown in **Figure 18**. Conversely, no change in the resonance is expected when the wire is inserted into a hole which corresponds to an electric field node—such as in the center and left and right edges—for the TE_{210} mode. When the wire is bent at a right angle and inserted into the cavity lid above an electric field antinode, no change is seen in the resonance. This is because the wire is now perpendicular to the electric field, and so no current is induced in the wire and no energy is lost in this way.

[1] A transverse electric mode may have no more than a single zero-index, and indices must be integers between 0 and 9, inclusive.

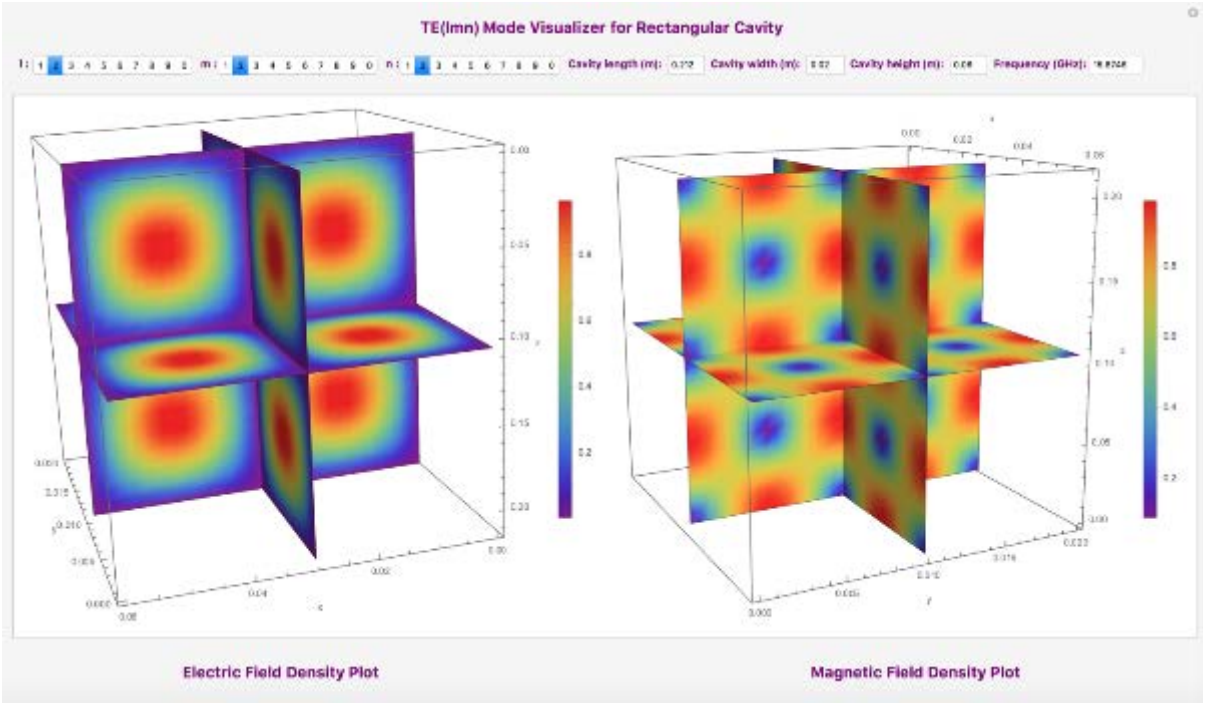

Figure 16

Interface of Mathematica program for visualizing TE modes in rectangular cavities using density plots of the electric and magnetic fields. Red regions correspond to high density areas, whereas blue regions correspond to low density areas. Pictured is the TE_{222} mode.

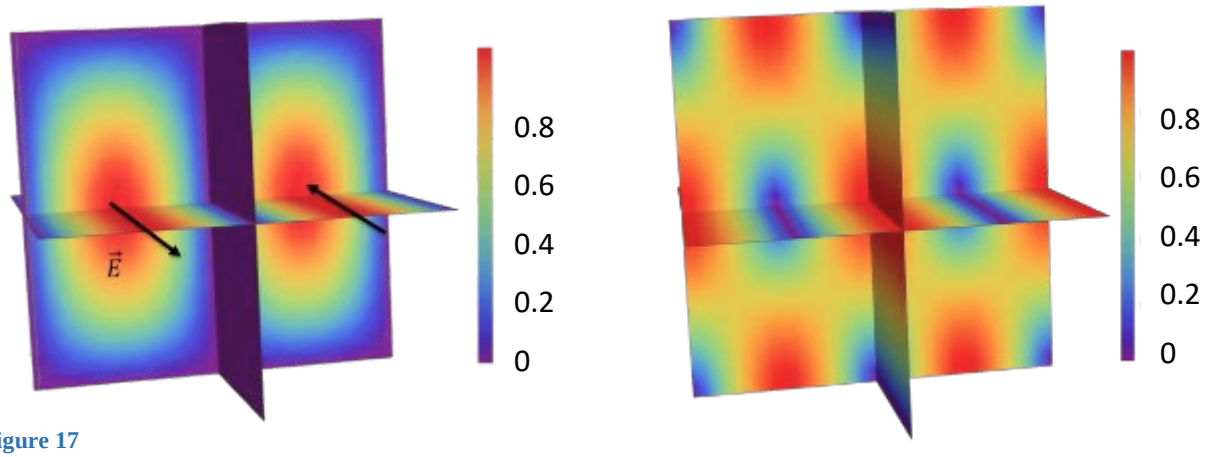

Figure 17

Visualization of TE_{210} mode using electric field density plot (left) and magnetic field density plot (right). Red regions correspond to high density areas, whereas blue regions correspond to low density areas.

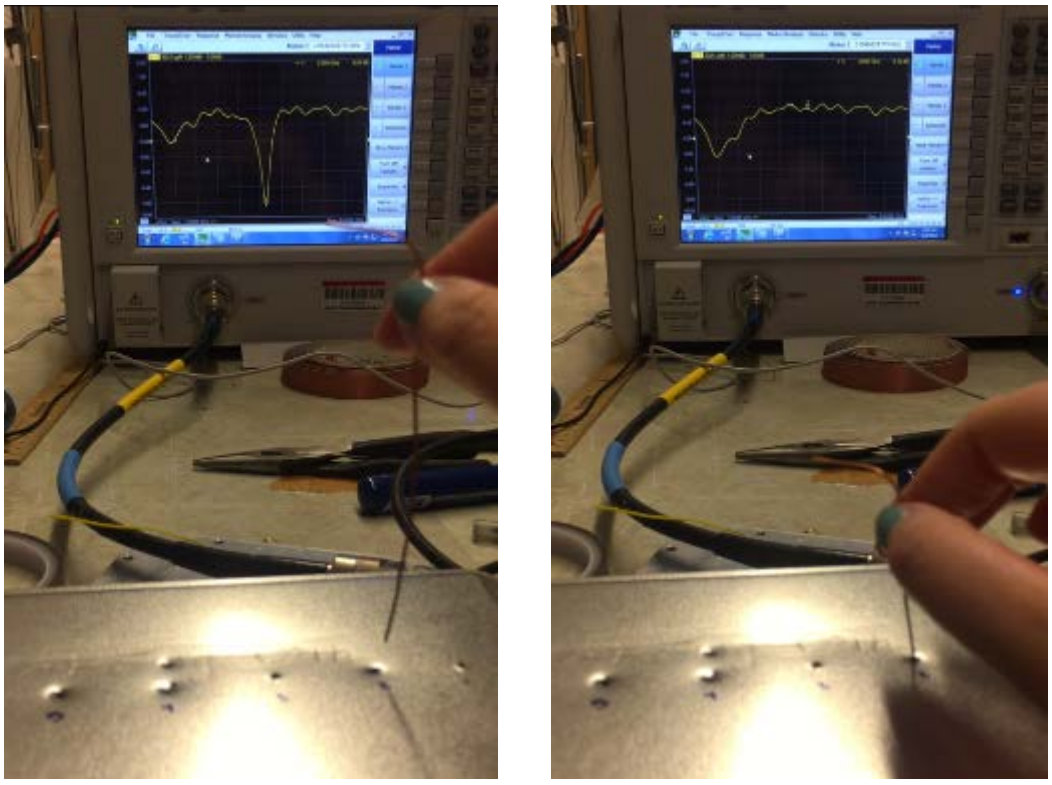

Figure 18

VNA network analyzer spectrum before and after probing the electric field of the TE_{210} mode with a copper wire inserted vertically into the cavity lid. This orientation of the wire is parallel with the electric field, which is transverse to the propagation direction. As a current is induced in the wire, energy is dissipated from the system, and the quality factor for the resonance is destroyed.

V. Final Cavity Design

The dimensions for the final cavity were set at length $d = 21.2$ cm, width $b = 2.0$ cm, and height $a = 6.0$ cm. For the cavity material, a highly conducting metal is desired. Ultimately, the chosen material was aluminum, which has fair conductivity and is much lower in

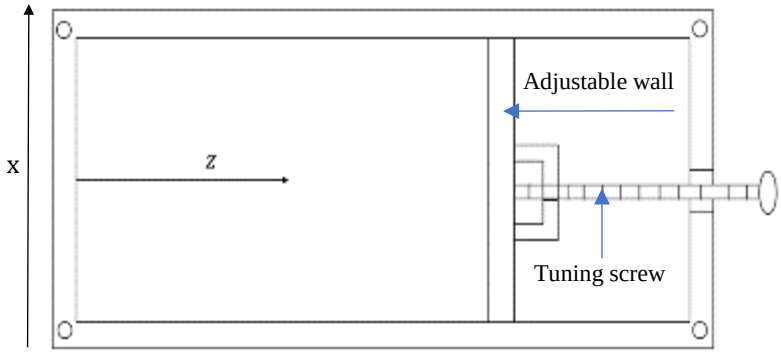

Figure 19

Original design of the microwave cavity.

cost than copper. This was a practical decision in the case that the resonance cavity did not function as desired. The cavity design (**Figure 19**) included an adjustable wall, such that the length of the cavity could be altered. This allowed for tuning of the cavity's resonance frequencies. Once the cavity was machined, probe holes were placed along the cavity lid.

V. RESULTS AND DISCUSSION

I. Model Microwave Cavity

Using the Java program and VNA data, each resonance for the model cavity could be matched with its corresponding modes. Data was collected for two loop orientations, vertical (XZ-plane), and horizontal (YZ-plane). For the loop oriented vertically (**Figure 20**), **Table 1** shows the observed resonance frequencies for the range 0-5 GHz. A sample of the frequency spectrum for this orientation is shown in (**Figure 21**).

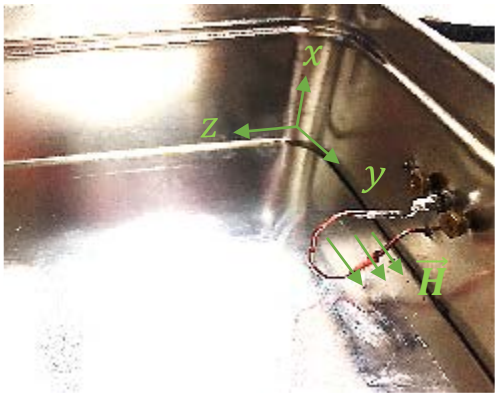

Figure 20

Vertical orientation of loop antenna in the model cavity. The direction of the magnetic field ($\mathbf{H}_1$) inside of the loop is shown.

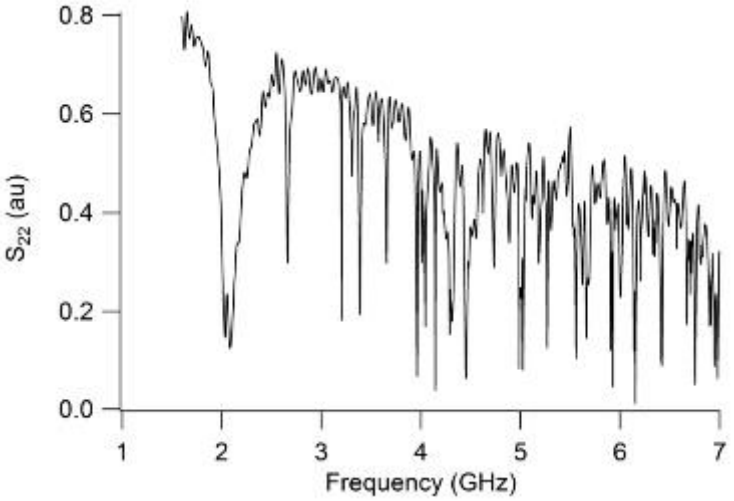

Figure 21

Spectrum generated by frequency sweep from VNA network analyzer, showing resonances from 0-7 GHz.

Table 1. Resonance frequencies observed for model cavity with vertical loop orientation from 0-7 GHz and corresponding transverse electric modes expected to contribute.

Frequency (GHz)	Modes (TE_{lmn})
2.995	110
3.221	014, 022, 102, 111
3.428	014, 112
3.684	113
3.981	015, 024, 104, 120, 121
4.229	031, 032, 114, 122
4.589	025, 033, 105, 123
4.625	016, 025, 033, 105, 123
4.805	016, 025, 033, 105, 115, 124, 130
5.025	124, 130, 131, 132
5.426	017, 026, 035, 041, 106, 116, 125, 133, 201
5.561	017, 035, 041, 042, 116, 125, 133, 201, 202, 210, 211
5.727	035, 042, 043, 134, 202, 203, 210, 211, 212
5.939	027, 036, 043, 107, 117, 126, 134, 140, 203, 212, 213, 220

II. Final Microwave Cavity

The original design of the microwave cavity included a circular loop of thin copper wire (**Figure 22**) for the antenna. The loop was oriented in the XZ-plane, with a diameter of 1.2cm. Resonances were observed in the frequency spectrum generated by the VNA at and near the desired frequency of 2.87GHz, but with poor Q-factors.

Figure 22

Original loop antenna diameter 1.2 cm oriented in XZ-plane of cavity for magnetic coupling between coaxial cable and microwave cavity.

Figure 23 shows a resonance at 2.873 GHz in the spectrum generated by a VNA frequency sweep. The FWHM was found to be approximately 6.1×10^6 GHz, for a Q-factor of about 471.

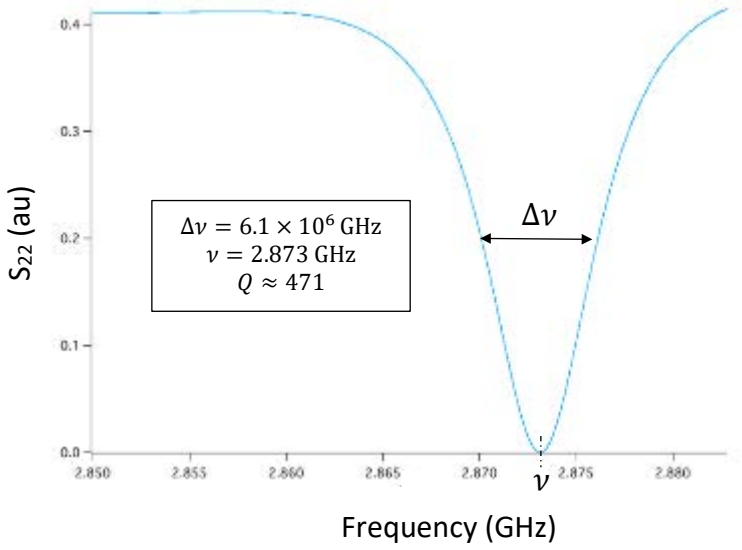

Figure 23

Resonance observed in VNA-generated spectrum at 2.873 GHz with 0-27 GHz frequency sweep for original loop antenna of one turn, with diameter1.2cm. The resonance yields a poor Q-factor, indicating unsatisfactory magnetic coupling between cavity and coaxial cable.

It was thought that the low Q-factor was due to poor coupling with the loop antenna, as it was constructed from thin wire that was easily deformed and difficult to keep in-plane. As the loop is turned out of the desired plane, the magnetic field lines generated by the loop lie at an angle to those circulating in the cavity, weakening the magnetic coupling by decreasing $H_1^{\parallel}$. To test this, a new loop antenna was constructed from thicker copper wire. The new antenna (**Figure 24**) consisted of two turns with an inner diameter of 0.9cm and an outer diameter of 1.3cm. It was thought that increasing the loop inductance would lead to stronger coupling between the coaxial cable and the cavity.

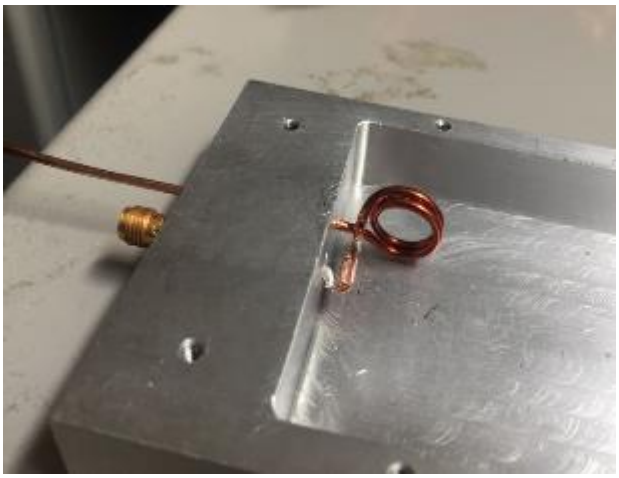

Figure 24

Coil antenna of two turns, inner diameter 0.9cm and outer diameter 1.3cm.

Figure 25 shows a strong resonance at 2.894 GHz in the spectrum generated by VNA frequency sweep. The FWHM was found to be approximately 2.9×10^6 GHz, for a Q-factor of about 998.

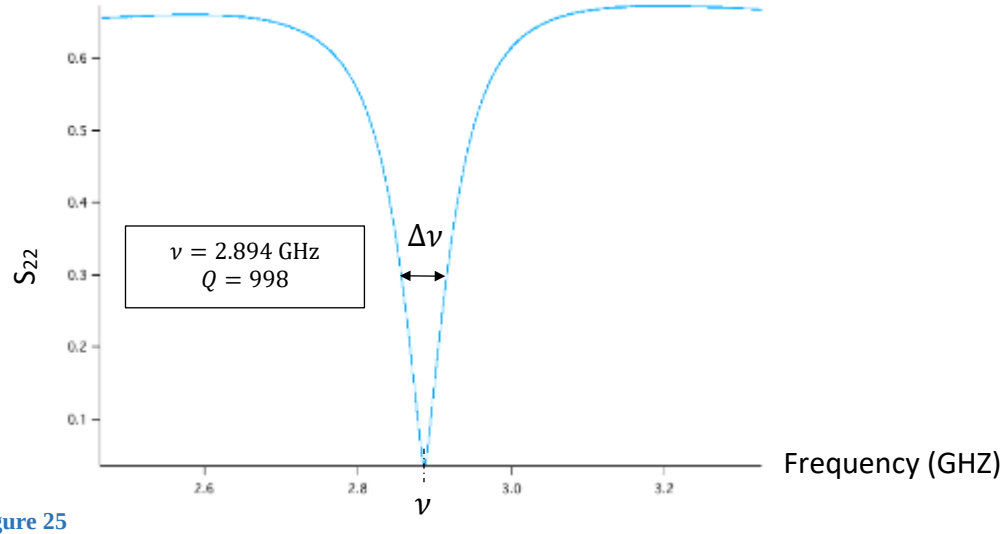

Figure 25

Resonance observed in VNA-generated spectrum at 2.894 GHz with 0-27 GHz frequency sweep for coil antenna of two turns, with inner diameter 0.9 cm. The resonance yields a better Q-factor than the original loop, indicating better magnetic coupling between cavity and coaxial cable.

Table 2 lists the first four resonances observed in the VNA frequency spectrum and the corresponding modes for this antenna. Each of the observed modes has $n = 0$ due to the loop orientation and resulting magnetic coupling. As the frequencies increase, the index l increases as well, which is not surprising as increasing frequencies indicate decreasing wavelengths. The cavity length is the longest dimension, and hence, a larger number of half wavelengths may be accommodated in this dimension.

Table 2. First four resonances produced by VNA frequency sweep for large coil antenna and corresponding transverse electric modes at a cavity length of 21.05cm.

Frequency (GHz)	Modes (TE_{lmn})
2.871	210
3.23	310
3.912	410
5.037	120, 220, 610

The coil antenna had a smaller diameter than the original loop antenna, and an extra turn. While the Q-factor improved, it was unclear as to which of these new features the increase could be attributed. Equation 2.6 indicates that the addition of a second turn should increase the coupling coefficient β. However, this would seem to insinuate that the cavity had been undercoupled before, yet undercoupling should result in a higher Q-factor (§1.2). However, the 25% decrease in loop diameter is expected to weaken the coupling, which may indicate that the cavity had previously been overcoupled instead, and the addition of the second loop did not increase the coupling so much as to prevent undercoupling. To determine which case was valid, a new loop antenna was constructed with two turns and a smaller diameter. This coil had an inner diameter of 0.495cm and an outer diameter of 0.851cm (**Figure 26**).

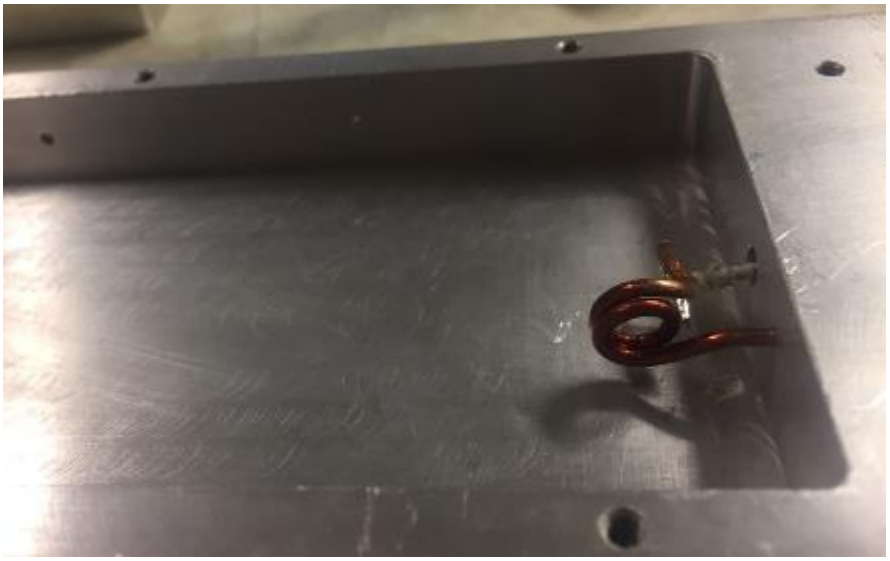

Figure 26

Coil antenna of two turns, inner diameter 0.495cm and outer diameter 0.851cm.

This smaller coil revealed a Q of just over 800 (**Figure 27**), indicating that a smaller coil diameter had somehow made the coupling less favorable. This was an unexpected result. A smaller loop diameter should weaken the coupling, thereby also lessening the power lost via the antenna, and increasing the Q-factor. It is unclear at this time why this result was observed, but it may be an anomaly. All data for the larger coil but one frequency was lost after it was replaced with the smaller coil, leaving only one available Q for comparison.

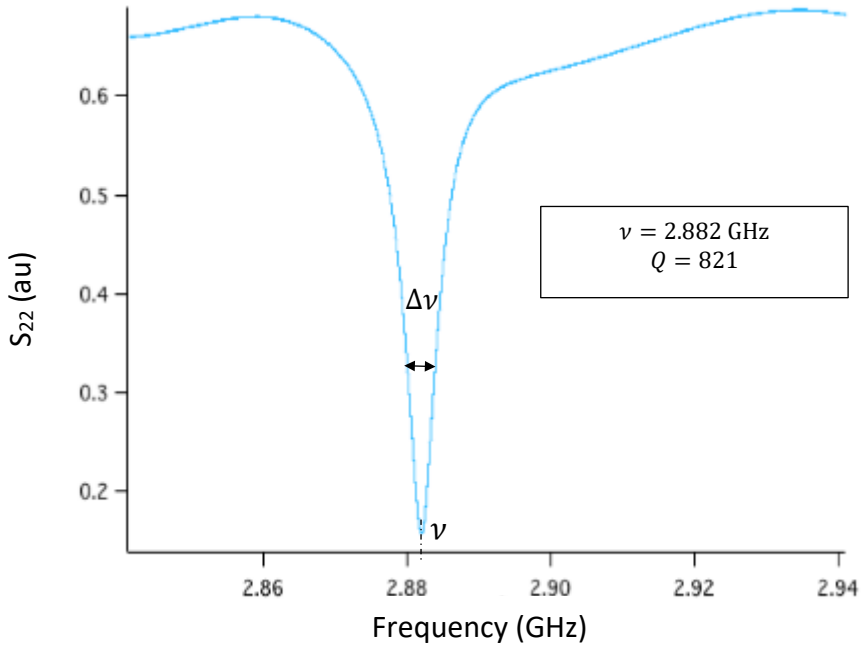

Figure 27

Resonance observed in VNA-generated spectrum at 2.882 GHz with 0-27 GHz frequency sweep for coil antenna of two turns, with inner diameter 0.495 cm.

Table 3 lists the first three resonances observed in the VNA frequency spectrum and the corresponding modes for this antenna. The modes progress as discussed for the first coil antenna above. It is observed that for this antenna, there are fewer resonances in the lower range of frequencies, perhaps indicating poor coupling.

Table 3. First three resonances produced by VNA frequency sweep for small coil antenna and corresponding transverse electric modes at a cavity length of 21.05cm.

Frequency (GHz)	**Modes (TE_{lmn})**
2.879	210
3.289	310
3.774	410

The last antenna to be tested was a loop of a single turn, now with an inner diameter of 0.509cm (42% of the original inner loop diameter) and an outer diameter of 0.822cm. This loop yielded the highest Q-factor of the four antennas at approximately 1314 (**Figure 28**). This result is expected, as the power loss via the antenna is proportional to $R_0 n^2$, indicating that a single turn will result in a higher Q. It is also known that a larger loop diameter leads to stronger coupling, and so a smaller loop diameter will help to inhibit overcoupling. It was therefore determined that the low Q of the original loop was due to the large loop diameter, likely resulting in an overcoupled cavity.

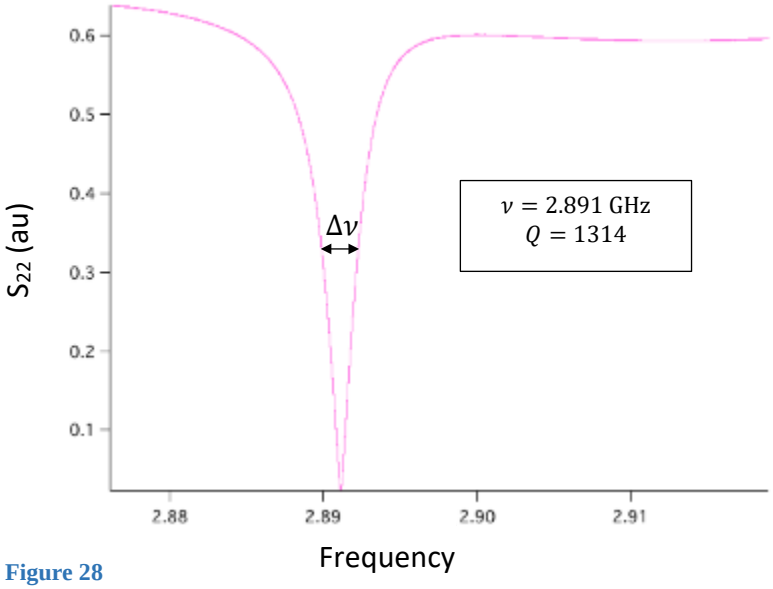

Figure 28

Resonance observed in VNA-generated spectrum at 2.894 GHz with 0-27 GHz frequency sweep for coil antenna of a single turn, with inner diameter 0.509 cm. The resonance yields a better Q-factor than any previous antenna, indicating more favorable magnetic coupling between cavity and coaxial cable.

Table 4 lists the first four resonances observed in the VNA frequency spectrum and the corresponding modes for this loop antenna. The modes progress as discussed for the coil antennas above.

Table 4. First four resonances produced by VNA frequency sweep for small loop antenna and corresponding transverse electric modes at a cavity length of 21.05cm.

Frequency (GHz)	Modes (TE_{lmn})
2.916	210
3.357	310
3.871	410
4.454	510

Upon tuning the cavity to the desired frequency and achieving a preliminarily reasonable Q-factor, the next step involved placing the microwave cavity into an external magnet with a nanodiamond sample inside and performing the magnetic resonance measurements. First, it was necessary to design holders for the cavity such that it would be kept flat and still within the magnet. These holders were ultimately 3-D printed, and are shown below in **Figure 29**.

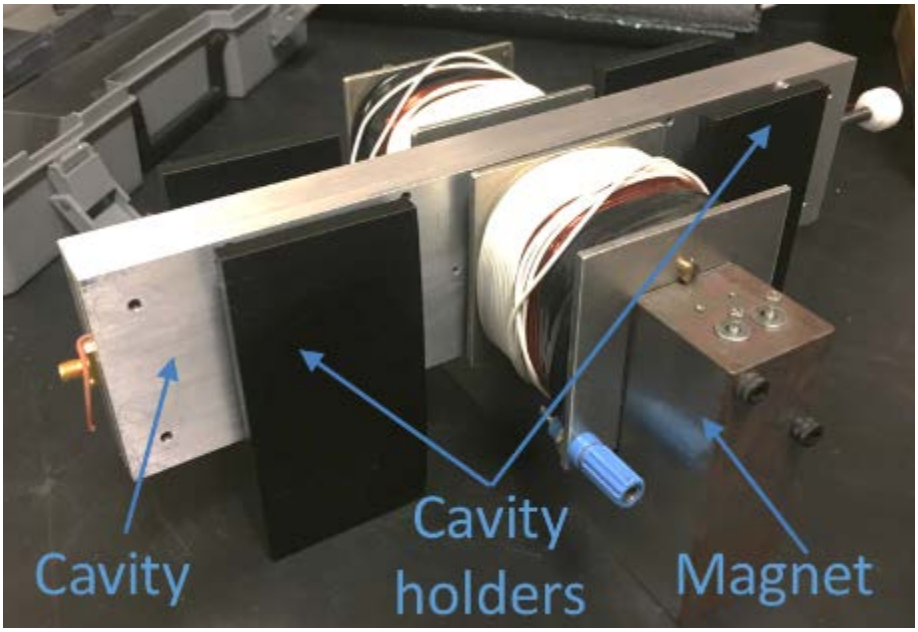

Figure 29

Experimental setup showing microwave cavity, cavity holders, and external electromagnet.

VI. CONCLUSION

In order to obtain EPR spectra which can be used to accurately determine the density of NV centers in a given nanodiamond sample, it is necessary to use a cavity which is tuned to a lower frequency than is typically available with commercial EPR cavities in order to avoid powder dispersions which distort EPR signals. A cavity tuned to the zero-field splitting of the nitrogen-vacancy center was developed, such that minimum magnetic field intensities are required during the external magnetic field sweep to achieve resonance, thereby decreasing the inclusion of the powder dispersions. The cavity includes an adjustable wall for fine tuning of the resonance, but is quite large relative to the typical EPR cavity, thus requiring larger samples. Future work will involve placing the cavity into an external electromagnet and performing a magnetic field sweep under a constant microwave frequency to obtain magnetic resonance measurements. These measurements are hoped to be of high enough quality that the NV density in an enclosed sample can be accurately quantified.

LITERATURE CITED

1. Schirhagl, Romana, et al. “Nitrogen-Vacancy Centers in Diamond: Nanoscale Sensors for Physics and Biology.” *Annual Review of Physical Chemistry*, vol. 65, no. 1, 2014, pp. 83–105., doi:10.1146/annurev-physchem-040513-103659.
2. Eaton, Gareth R., et al. “Resonator Q.” *Quantitative EPR*, 2010, pp. 79–87., doi:10.1007/978-3-211-92948-3_7.
3. Eaton, Gareth R., et al. “Filling Factor.” *Quantitative EPR*, 2010, pp. 89–90., doi:10.1007/978-3-211-92948-3_8.
4. (reference for over and under coupling)
5. Griffiths, David J. *Introduction to Electrodynamics*. 4th ed., Pearson, 2014.
6. Teeling-Smith, Richelle M., and P. Chris Hammel. “Single Molecule Electron Paramagnetic Resonance and Other Sensing and Imaging Applications with Nitrogen-Vacancy Nanodiamond.” *The Ohio State University*, 2015, pp. 87.
7. “NV9.” MIZUOCHI Laboratory, Institute for Chemical Research, Kyoto University, n.d., http://mizuochilab.kuicr.kyoto-u.ac.jp/image/NV9.png
8. Bruker Biospin.“Basic Concepts of EPR Resonators,” n.d.